Available online at www.sciencedirect.com
SCIENCE DIRECT®
Journal of Solid State Chemistry 178 (2005) 1017–1022
JOURNAL OF SOLID STATE CHEMISTRY
www.elsevier.com/locate/jssc

High-temperature, high-pressure hydrothermal synthesis and characterization of a new framework stannosilicate: $Cs_2SnSi_3O_9$

Fang-Rey Lo[a], Kwang-Hwa Lii[a,b,*]

[a]*Institute of Chemistry, Academia Sinica, Nankang, Taipei, Taiwan 115, ROC*
[b]*Department of Chemistry, National Central University, Number 300, Junda Road, Chungli, Taiwan 320, ROC*

Received 29 September 2004; received in revised form 29 November 2004; accepted 2 December 2004

Abstract

A new stannosilicate $Cs_2SnSi_3O_9$ has been synthesized and characterized by single-crystal X-ray diffraction and solid-state NMR spectroscopy. It crystallizes in the orthorhombic space group $P2_12_12_1$ (No. 19) with $a = 7.9612(7)$ Å, $b = 10.3444(9)$ Å, $c = 11.780(1)$ Å, $V = 970.1(3)$ Å^3, and $Z = 4$ with $R_1 = 0.0189$. The structure consists of helical silicate chains with a period of six tetrahedra which are connected by SnO_6 octahedra to form a 3D framework containing 6-ring and 7-ring channels where the Cs^+ cations reside. This work is one of the few studies concerning the synthesis of stannosilicates under high-temperature and high-pressure hydrothermal conditions.

Keywords: Silicate; Tin; Hydrothermal; Crystal structure; Solid-state NMR

1. Introduction

Hydrothermal synthesis of microporous framework silicates possessing structures, which consist of interlinked octahedra and tetrahedra has been the subject of considerable interest [1]. A large number of studies has been concerned with the chemistry of titanium and zirconium silicates containing tetrahedral Si^{4+} and Ti^{4+} or Zr^{4+} usually in octahedral coordination. Recently this research was extended to stannosilicates. Several small-pore framework stannosilicates with the general formula $A_2SnSi_3O_9 \cdot nH_2O$ have been reported. $K_2SnSi_3O_9 \cdot H_2O$ (named AV-6) [2] adopts the structure of the rare mineral umbite ($K_2ZrSi_3O_9 \cdot H_2O$) [3–5]. A new potassium stannosilicate, $K_2SnSi_3O_9$ (AV-11), was synthesized by calcining AV-6 in air at high temperature [6]. Both AV-6 and AV-11 contain infinite chains of corner-sharing SiO_4 tetrahedra. However, in the structure of AV-6 the infinite chain has a period of three tetrahedra, while in the structure of AV-11 the chain has a period of six tetrahedra. These infinite chains are connected by SnO_6 octahedra in different ways in the two structures. Interestingly, $K_2SnSi_3O_9$ which was prepared by high-temperature solid-state reaction of SnO_2, SiO_2, and K_2CO_3 adopts wadeite-type structure [7]. In the structure of wadeite the SiO_4 tetrahedra form three-membered rings, which are connected by MO_6 octahedra. Thus, umbite and wadeite have entirely different structures. The sodium stannosilicate $Na_2SnSi_3O_9 \cdot 2H_2O$ (AV-10) has a new structure [8]. Although both AV-10 and AV-11 contain infinite silicate chains with a period of six tetrahedra, the chains are connected by SnO_6 octahedra in different ways. A sodium chloride stannosilicate, $Na_{2.26}SnSi_3O_9Cl_{0.26} \cdot xH_2O$ (AV-13), was reported and its 3D framework structure consists of six-membered $[Si_6O_{18}]^{12-}$ rings, which are interconnected by SnO_6 octahedra [9]. All the stannosilicates in the AV-*n* family were synthesized under hydrothermal conditions in a Teflon-lined autoclave at 200–230 °C and

*Corresponding author. Department of Chemistry, National Central University, Number 300, Junda Road, Chungli, Taiwan 32054, ROC. Fax: +886 3 422 7664.
E-mail address: liikh@cc.ncu.edu.tw (K.-H. Lii).

0022-4596/$ - see front matter © 2004 Elsevier Inc. All rights reserved.
doi:10.1016/j.jssc.2004.12.002

structurally characterized by powder X-ray diffraction due to the lack of single crystals. In this paper, we report high-temperature, high-pressure hydrothermal synthesis and single-crystal X-ray structure of a cesium stannosilicate, $Cs_2SnSi_3O_9$. It adopts a structure similar to the sodium stannosilicate AV-10, but they crystallize in different space groups. The title compound has also been studied by solid-state NMR spectroscopy and second harmonic generation measurement.

2. Experimental

2.1. Synthesis and initial characterization

The hydrothermal reactions were carried out under autogenous pressure in gold ampules contained in a Leco Tem-Pres autoclave, where pressure was provided by water. The degree of filling of the autoclave by water at room temperature is 60%. A reaction mixture of $CsOH_{(aq)}$ (Acros, 50 wt% in water, 99%), SnO_2 (Aldrich, 99.9%), and SiO_2 (Alfa Aesar, 99.995%) (molar ratio Cs:Sn:Si = 7:1:4) in a 6 cm long gold ampule (inside diameter = 4.85 mm) was heated at 610 °C for 5*d*. The pressure was estimated to be 210 MPa according to the pressure–temperature diagram of pure water. The autoclave was then cooled to 300 °C at 5 °C/h followed by fast cooling to room temperature by removing the autoclave from the furnace. The product contained colorless crystals and powder. EDX analysis of several crystals confirmed the presence of Cs, Sn, and Si. A crystal was selected for structure determination by single-crystal X-ray diffraction. Powder X-ray data were collected on a Shimadzu XRD-6000 automated powder diffractometer with Cu $K\alpha$ radiation equipped with a scintillation detector. Data were collected in the range of $5^\circ \le 2\theta \le 50^\circ$ using $\theta-2\theta$ mode in a Bragg–Brentano geometry. The bulk product was a single phase of $Cs_2SnSi_3O_9$, **1**, because its powder pattern is in good agreement with the calculated pattern based on the results from single-crystal X-ray diffraction (Fig. 1). The program XPOW in the SHELXTL version 5.1 software package was used for XRPD simulation [10]. The yield was 78% based on tin. The sample was used for solid-state NMR spectroscopy measurements. TGA and infrared spectroscopy did not reveal any lattice water in the sample.

Crystals of $K_2SnSi_3O_9$ and $Rb_2SnSi_3O_9$ have also been obtained from hydrothermal reactions of $AOH_{(aq)}$ (A = K, Rb), SnO_2, and SiO_2 under analogous conditions. They adopt wadeite-type structure, as indicated from single-crystal X-ray diffraction. Crystal data: $K_2SnSi_3O_9$, $P6_3/m$ (No. 176), $a = 6.867(1)$ Å, $c = 10.024(2)$ Å, $R_1 = 0.0245$; $Rb_2SnSi_3O_9$, $P6_3/m$ (No. 176), $a = 6.982(1)$ Å, $c = 10.046(2)$ Å, $R_1 = 0.0237$.

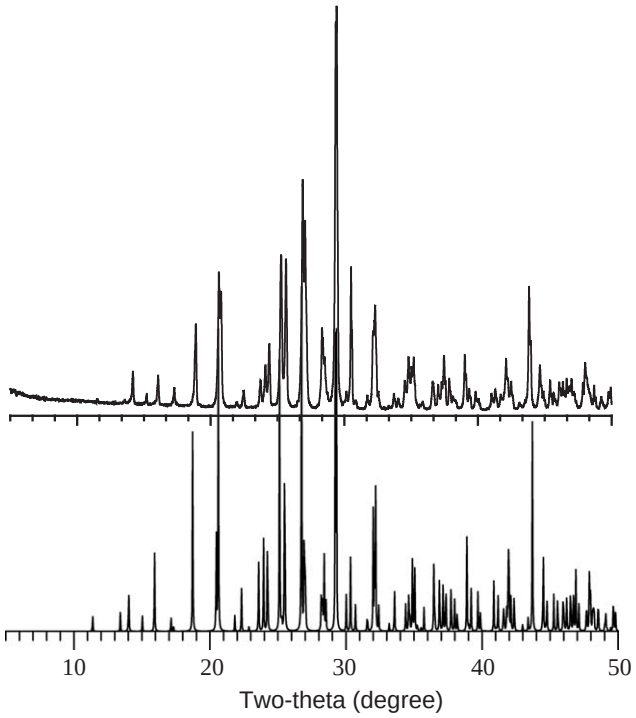

Fig. 1. Experimental X-ray powder pattern (top) and simulated powder pattern based on the results from single-crystal X-ray diffraction (bottom) for **1**.

These results are in good agreement with those by Choisnet et al. [7].

The second harmonic generation (SHG) response of powder $Cs_2SnSi_3O_9$ was measured. The sample was spread on a double-sided tape on a glass plate. A pulsed Nd:YAG laser operating at 1064 nm was used as the radiation source. The sample had a SHG signal about the same as that of quartz, confirming the absence of the center of symmetry in the structure.

2.2. Single-crystal X-ray diffraction

A suitable crystal of **1** with dimensions $0.08 \times 0.08 \times 0.05$ mm^3 was selected for indexing and intensity data collection on a Siemens SMART CCD diffractometer equipped with a normal focus, 3-kW sealed tube X-ray source. Intensity data were collected at room temperature in 1271 frames with ω scans (width 0.30° per frame). The program SADABS was used for the absorption correction ($T_{\min/\max} = 0.585/0.984$) [11]. The structure was solved by direct methods and difference Fourier syntheses. The final cycles of least-squares refinement included atomic coordinates and anisotropic thermal parameters for all atoms. The final difference Fourier maps were flat ($\Delta\rho_{\max,\min} = 0.55, -0.57$ e/Å^3). The Flack x parameter was $-0.02(2)$, indicative of a correct absolute structure. All calculations were performed using the SHELXTL Version 5.1 software package. Further details of the crystal structure investigation can

be obtained from the Fachinformationszentrum Karlsruhe, 76344 Eggenstein-Leopoldshafen, Germany (fax: +49-7247-808-666; *e-mail*: crysdata@fiz.karlsruhe.de) on quoting the depository number CSD-414425.

2.3. Solid-state NMR measurements

All NMR spectra were acquired on a Bruker AVANCE-400 spectrometer, operating at 79.46, 52.49, and 149.21 MHz for ^{29}Si, ^{133}Cs, and ^{117}Sn nuclei, respectively. A Bruker probe equipped with 4 mm rotors was used. ^{29}Si, ^{133}Cs, and ^{117}Sn MAS (magic angle spinning) NMR spectra were recorded with 30°, 15°, and 30° pulses, a spinning rate of 5, 10, and 10 kHz, and a recycle delay of 60, 1, and 80 s, respectively. The chemical shifts were externally referenced to TMS for ^{29}Si NMR, aqueous CsCl solution for ^{133}Cs NMR, and tetrabutyltin ($\delta = -13$ ppm) for ^{119}Sn NMR.

3. Results and discussion

3.1. Description of the structure

The crystal data and structure refinement parameters are given in Table 1, atomic coordinates and thermal parameters in Table 2, and selected bond lengths and bond valence sums [12] in Table 3. As shown in Fig. 2, the structure of **1** is constructed from the following structural elements: 3 SiO_4 tetrahedra, 1 $Sn^{IV}O_6$ octahedron, and 2 Cs sites. All atoms are at general positions. The observed Si–O bond lengths (1.595–1.646 Å, average 1.622 Å) and O–Si–O bond angles (102.4–115.3°) are typical values and are within the normal range [13]. Each SiO_4 tetrahedron shares two corners with other tetrahedra to form helical chains extending along the *c*-axis. All oxygen atoms in the chain except the three bridging atoms O_{br} linking two Si atoms, O(1), O(4), and O(6), are terminal atoms O_{term}

Table 1
Crystallographic data for $Cs_2SnSi_3O_9$

Formula	$Cs_2O_9Si_3Sn$
M	612.78
Crystal system	Orthorhombic
Space group	$P2_12_12_1$ (No. 19)
a (Å)	7.9612(7)
b (Å)	10.3444(9)
c (Å)	11.780(1)
V (Å^3)	970.1(3)
Z	4
T (K)	296
λ (Mo$K\alpha$) (Å)	0.71073
D_{calc} (g/cm^3)	4.196
μ (Mo$K\alpha$) (cm^{-1})	104.3
Measured reflections	7296
Unique reflections (R_{int})	2398 (0.0336)
Observed reflections [$I > 2\sigma(I)$]	2302
R_1[a]	0.0189
wR_2[b]	0.0350

[a] $R_1 = \sum ||F_o| - |F_c|| / \sum |F_o|$.

[b] $wR_2 = \sum\{[w(F_o^2 - F_c^2)^2] / \sum [w(F_o^2)^2]\}^{1/2}$, $w = 1/[\sigma^2(F_o^2) + (aP)^2 + bP]$, $P = [\mathrm{Max}(F_o, 0) + 2(F_c)^2]/3$, where $a = 0.0111$ and $b = 0$.

Table 2
Atomic coordinates and thermal parameters (Å^2) for $Cs_2SnSi_3O_9$

Atom	x	y	z	U_{eq}[a]
Cs(1)	0.26611(4)	−0.28848(3)	0.10250(3)	0.01745(8)
Cs(2)	−0.07570(4)	−0.10685(3)	0.52098(3)	0.01942(8)
Sn(1)	0.24517(4)	0.09024(3)	0.26362(2)	0.00711(7)
Si(1)	0.0790(2)	0.3898(1)	0.2914(1)	0.0084(2)
Si(2)	0.0849(2)	0.0250(1)	0.0072(1)	0.0082(2)
Si(3)	0.4402(2)	0.3734(1)	0.2140(1)	0.0080(2)
O(1)	0.2588(4)	0.4420(3)	0.2414(3)	0.0129(6)
O(2)	−0.0677(4)	0.4496(3)	0.2156(3)	0.0140(7)
O(3)	0.0808(4)	0.2350(3)	0.2995(3)	0.0130(7)
O(4)	0.0585(4)	0.4440(3)	0.4216(2)	0.0132(7)
O(5)	0.1927(3)	0.1115(3)	0.0936(2)	0.0106(6)
O(6)	−0.0295(4)	0.1164(3)	−0.0766(2)	0.0124(7)
O(7)	0.1951(4)	−0.0723(3)	−0.0681(2)	0.0122(7)
O(8)	0.4339(4)	0.2230(3)	0.2471(3)	0.0111(6)
O(9)	0.5839(4)	0.4496(3)	0.2810(2)	0.0119(7)

[a] U_{eq} is defined as one-third of the trace of the orthogonalized U_{ij} tensor.

Table 3
Bond lengths (Å) and bond valence sums ($\sum s$) for $Cs_2SnSi_3O_9$

Cs(1)–O(8)^{i}	2.976(3)	Cs(1)–O(3)^{ii}	3.003(3)
Cs(1)–O(4)^{iii}	3.013(3)	Cs(1)–O(7)	3.059(3)
Cs(1)–O(9)^{i}	3.062(3)	Cs(1)–O(1)^{iv}	3.233(3)
Cs(1)–O(4)^{ii}	3.541(3)	Cs(1)–O(2)^{ii}	3.627(3)
$\sum s$(Cs(1)–O) = 1.17			
Cs(2)–O(6)^{ii}	3.054(3)	Cs(2)–O(2)^{ii}	3.068(3)
Cs(2)–O(9)^{v}	3.114(3)	Cs(2)–O(8)^{vi}	3.132(3)
Cs(2)–O(5)^{vi}	3.167(3)	Cs(2)–O(5)^{ii}	3.343(3)
Cs(2)–O(6)^{vii}	3.348(3)	Cs(2)–O(4)^{v}	3.342(3)
Cs(2)–O(1)^{ii}	3.454(3)	Cs(2)–O(1)^{v}	3.533(3)
$\sum s$(Cs(2)–O) = 1.12			
Sn(1)–O(3)	2.033(3)	Sn(1)–O(2)^{ii}	2.060(3)
Sn(1)–O(8)	2.045(3)	Sn(1)–O(7)^{vi}	2.047(3)
Sn(1)–O(5)	2.058(3)	Sn(1)–O(9)^{i}	2.060(3)
$\sum s$(Sn(1)–O) = 4.08			
Si(1)–O(2)	1.595(3)	Si(1)–O(3)	1.604(3)
Si(1)–O(1)	1.640(3)	Si(1)–O(4)	1.641(3)
$\sum s$(Si(1)–O) = 4.23			
Si(2)–O(7)	1.603(3)	Si(2)–O(5)	1.604(3)
Si(2)–O(6)	1.642(3)	Si(2)–O(4)^{ii}	1.646(3)
$\sum s$(Si(2)–O) = 4.19			
Si(3)–O(9)	1.598(3)	Si(3)–O(8)	1.604(3)
Si(3)–O(6)^{viii}	1.640(3)	Si(3)–O(1)	1.641(3)
$\sum s$(Si(3)–O) = 4.22			

Symmetry codes: (i) $-x+1$, $y-1/2$, $-z+1/2$; (ii) $-x$, $y-1/2$, $-z+1/2$; (iii) $-x+1/2$, $-y$, $z-1/2$; (iv) x, $y-1$, z; (v) $x-1/2$, $-y+1/2$, $-z+1$; (vi) $-x+1/2$, $-y$, $z+1/2$; (vii) $-x-1/2$, $-y$, $z+1/2$; (viii) $x+1/2$, $-y+1/2$, $-z$.

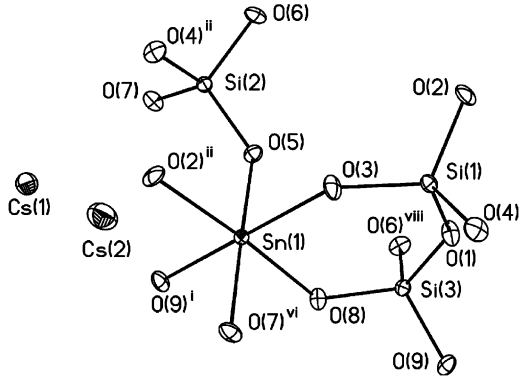

Fig. 2. Building units of 1 showing atom labeling scheme. Thermal ellipsoids are shown at 50% probability.

which coordinate to Sn atoms. The Si–O_{br}–Si angles are 134.2, 136.0 and 135.4° for O(1), O(4) and O(6), respectively, which are within the normal range and comparable with the angles in the AV-*n* family. All oxygen atoms coordinate to Cs atoms. The SnO_6 octahedron is regular with the Sn–O bond lengths in the range from 2.033 to 2.060 Å. Each SnO_6 octahedron shares its corners with six SiO_4 tetrahedra. Both Cs sites are fully occupied. Based on the maximum cation–anion distance by Donnay and Allmann [14], a limit of 3.70 Å was set for Cs–O interactions, which gives the following coordinations: Cs(1) has 6 neighboring oxygen atoms at distances of 2.976–3.233 Å and two others at 3.541 and 3.627 Å; Cs(2) has 10 neighboring oxygen atoms at 3.054–3.533 Å. The atomic displacement factors for both Cs atoms are regular and normal, indicating that they are not loosely bound in the structural channels.

The structure of **1** consists of helical silicate chains with a period of six tetrahedra which are connected by SnO_6 octahedra to form a 3D framework structure (Fig. 3a). Each SnO_6 octahedron connects to six SiO_4 tetrahedra which belong to three different chains. Each chain connects two SiO_4 tetrahedra to a SnO_6 octahedron. In this way, two distinct 6-ring channels are formed along the [100] direction. Cs(1) atom is located near the center of one channel, whereas Cs(2) is near the wall of the other channel. These channels have lateral windows which are aligned such that 7-ring channels are formed along the [101] and [110] directions. A slice of the structure in the *ac*-plane contains 8-membered rings formed by 6 tetrahedra and 2 octahedra (Fig. 3b), but the 8-rings are not aligned to form straight channels. The structure of **1** is similar to that of $Na_2SnSi_3O_9 \cdot 2H_2O$ (AV-10) which crystallizes in a different orthorhombic space group $C222_1$ and contains lattice water in the structural channels [8]. In the structure of AV-10 the Sn, one Si, and both Na atoms have a local symmetry of C_2. In contrast, all atoms in **1** are at general positions. In AV-10 the water molecules are located in the 6-ring channels such that the Na atoms shift to sites

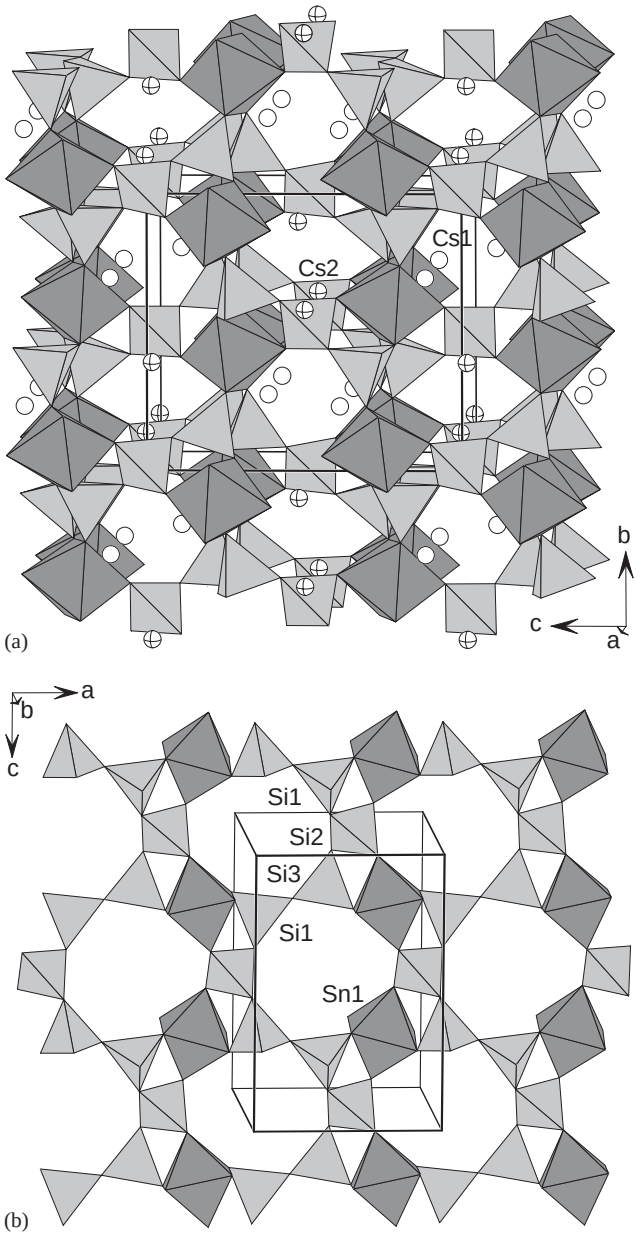

Fig. 3. (a) Structure of 1 viewed along the *a*-axis. The medium gray and light gray polyhedra are SnO_6 octahedra and SiO_4 tetrahedra, respectively. Open circles without and with a cross are Cs(1) and Cs(2) atoms, respectively. (b) Slice of the structure of 1 showing the silicate chains and the connectivity between the chains and SnO_6 octahedra.

between channels. The Na atoms are coordinated by framework oxygens and water molecules. In addition, the silicate chain helix turns clockwise in AV-10 and counterclockwise in **1**.

3.2. ^{29}Si, ^{133}Cs and ^{119}Sn MAS NMR

The ^{29}Si MAS NMR spectrum of **1** (Fig. 4a) displays two peaks at −89.2 and −90.2 ppm in a 2:1 intensity ratio. It has been reported that the ^{29}Si chemical shift depends on the average value of the four Si–O–T bond

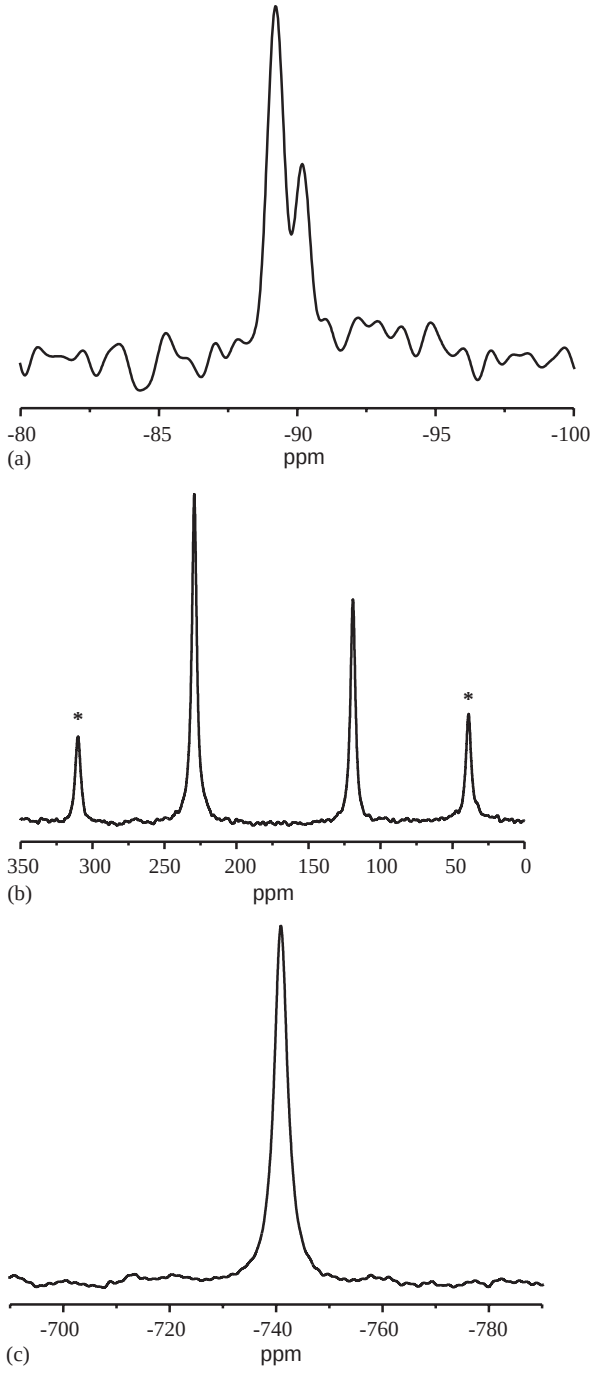

Fig. 4. (a) ^{29}Si, (b) ^{133}Cs, and (c) ^{119}Sn MAS NMR spectrum of **1**.

angles (two Si–O–Si angles and two Si–O–Sn angles for each silicon) and shifts upfield with increasing Si–O–T bond angle [15]. The average Si–O–T bond angles in **1** are 135.7°, 134.8°, and 134.5° for Si(1), Si(2), and Si(3), respectively. The angles for Si(2) and Si(3) are close and are significantly smaller than that for Si(1). The peak at −90.2 ppm is therefore assigned to Si(1) and the other peak to Si(2) and Si(3). For comparison the ^{29}Si MAS NMR spectrum of AV-10 shows two peaks at −87.0 and −88.7 ppm. Other reported framework stannosilicates give resonances in the range of −78 to −92 ppm [16,17]. The ^{133}Cs MAS NMR spectrum of **1** (Fig. 4b) displays two sharp peaks at 229.3 and 119.1 ppm assuming that the contribution of the second-order quadrupolar shift is small. The sidebands were determined by varying the spinning speed. The two peaks correspond to two unique Cs sites as determined from X-ray diffraction. ^{133}Cs in inorganic cesium compounds shows a moderate chemical shift range of about 300 ppm [18]. The ^{133}Cs chemical shift is expected to decrease with increasing oxygen coordination number (CN) resulting from increased shielding. Therefore, the 119.1 ppm peak in the spectrum of **1** corresponds to more highly coordinated Cs(2) (CN = 10), and the 229.3 ppm peak corresponds to Cs(1) (CN = 6 + 2). The peak intensities do not seem to be in a 1:1 ratio because ^{133}Cs is a quadrupolar nuclei ($I = 7/2$). The ^{119}Sn MAS NMR spectrum of **1** displays a single peak at −740 ppm, which corresponds to the single Sn(6Si) environment in the structure. For comparison the ^{119}Sn MAS NMR spectrum of AV-10 shows a single peak at ca. −706 ppm.

3.3. Concluding remarks

This work reports high-temperature, high-pressure hydrothermal synthesis and structural characterization by single-crystal X-ray diffraction and solid-state NMR spectroscopy of a new stannosilicate. $Cs_2SnSi_3O_9$ adopts a structure similar to that of the sodium stannosilicate AV-10 which was prepared under mild hydrothermal conditions, but the two compounds crystallize in different space groups. The 3D framework structure of **1** consists of helical silicate chains with a period of six tetrahedra which are connected by SnO_6 octahedra to generate 6-ring and 7-ring channels where the Cs^+ cations are located. There are some previous reports describing the synthesis of stannosilicates by hydrothermal growth at high temperatures [19,20]. Subsequent studies have concentrated on mild hydrothermal reactions to synthesize microporous stannosilicates, but their structures have been characterized only by powder X-ray diffraction. The high-temperature, high-pressure hydrothermal method is especially useful for the crystal growth of metal silicates. For example, millimeter-sized sodalite single crystals can be grown by the method [21]. Given a variety of metal cations that could be used in the hydrothermal synthesis, the scope for the synthesis of new stannosilicates with interesting structures appears to be very large.

Acknowledgments

We thank the National Science Council for support, Ms. F.-L. Liao and Prof. S.-L. Wang at National Tsing

Hua University for X-ray data collection, Prof. B.-C. Chang at National Central University for SHG measurements, Ms. R.-R. Wu at National Cheng Kung University for NMR spectra measurements, and Prof. H.-M. Kao at National Central University for helpful discussions.

References

[1] J. Rocha, M.W. Anderson, Eur. J. Inorg. Chem. 5 (2000) 801 and references therein.
[2] Z. Lin, J. Rocha, A. Valente, Chem. Commun. 24 (1999) 2489.
[3] V.V. Ilyukhin, Z.V. Pudovkina, A.A. Voronkov, A.P. Khomyakov, J.A. Pyatenko, Dokl. Akad. Nauk SSSR 257 (1981) 608.
[4] D.M. Poojary, A.I. Bortun, L.N. Bortun, A. Clearfield, Inorg. Chem. 36 (1997) 3072.
[5] Z. Lin, J. Rocha, P. Ferreira, A. Thursfield, J.R. Agger, M. Anderson, J. Phys. Chem. B 103 (1999) 957.
[6] Z. Lin, A. Ferreira, J. Rocha, J. Solid State Chem. 175 (2003) 258.
[7] J. Choisnet, A. Deschanvres, B. Raveau, J. Solid State Chem. 7 (1973) 408.
[8] A. Ferreira, Z. Lin, J. Rocha, C.M. Morais, M. Lopes, C. Fernandez, Inorg. Chem. 40 (2001) 3330.
[9] A. Ferreira, Z. Lin, M.R. Soares, J. Rocha, Inorg. Chim. Acta 356 (2003) 19.
[10] G.M. Sheldrick, SHELXTL Programs, Version 5.1, Bruker AXS GmbH: Karlsruhe, Germany, 1998.
[11] G.M. Sheldrick, SADABS, Program for Siemens Area Detector Absorption Corrections, University of Göttingen, Germany, 1997.
[12] I.D. Brown, D. Altermatt, Acta Crystallogr. B 41 (1985) 244.
[13] F. Liebau, Structural Chemistry of Silicates: Structure, Bonding and Classification, Springer, Berlin, 1985.
[14] G. Donnay, R. Allmann, Am. Mineral. 55 (1970) 1003.
[15] R. Radeglia, G. Engelhardt, Chem. Phys. Lett. 114 (1985) 28.
[16] E.W. Corcoran Jr., D.E.W. Vaughan, Solid State Ionics 32/33 (1989) 423.
[17] A. Dyer, J.J. Jafar, J. Chem. Soc. Dalton Trans. 11 (1990) 3239.
[18] K.J.D. MacKenzie, M.E. Smith, Multinuclear Solid-State NMR of Inorganic Materials, Elsevier Science, Oxford, 2002.
[19] N.V. Zayakina, I.V. Rozhdestvenskaya, I.Y. Nekrasov, T.P. Dadze, Dokl. Akad. Nauk SSSR 254 (1980) 353.
[20] A.N. Safronov, N.N. Nevskii, V.V. Ilyukhin, N.V. Belov, Dokl. Akad. Nauk SSSR 269 (1983) 850.
[21] T. Shiraki, T. Wakihara, M. Sadakata, M. Yoshimura, T. Okubo, Micrpor. Mesopor. Mater. 42 (2001) 229.